

Trace rare gases optical emission spectroscopy: Nonintrusive method for measuring electron temperatures in low-pressure, low-temperature plasmas

M. V. Malyshev and V. M. Donnelly

Bell Laboratories, Lucent Technologies, Murray Hill, New Jersey 07974

(Received 10 June 1999)

Trace rare gases optical emission spectroscopy (TRG-OES) is a new, nonintrusive method for determining electron temperatures (T_e) and, under some conditions, estimating electron densities (n_e) in low-temperature, low-pressure plasmas. The method is based on a comparison of atomic emission intensities from trace amounts of rare gases (an equimixture of He, Ne, Ar, Kr, and Xe) added to the plasma, with intensities calculated from a model. For Maxwellian electron energy distribution functions (EEDFs), T_e is determined from the best fit of theory to the experimental measurements. For non-Maxwellian EEDFs, T_e derived from the best fit describes the high-energy tail of the EEDF. This method was reported previously, and was further developed and successfully applied to several laboratory and commercial plasma reactors. It has also been used in investigations of correlations between high- T_e and plasma-induced damage to thin gate oxide layers. In this paper, we provide a refined mechanism for the method and include a detailed description of the generation of emission from the Paschen $2p$ manifold of rare gases both from the ground state and through metastable states, a theoretical model to calculate the number density of metastables (n_m) of the rare gases, a practical procedure to compute T_e from the ratios of experimental-to-theoretical intensity ratios, a way to determine the electron density (n_e), a discussion of the range of sensitivity of TRG-OES to the EEDF, and an estimate of the accuracy of T_e . The values of T_e obtained by TRG-OES in a transformer-coupled plasma reactor are compared with those obtained with a Langmuir probe for a wide range of pressures and powers. The differences in T_e from the two methods are explained in terms of the EEDF dependence on pressure. [S1063-651X(99)14111-4]

PACS number(s): 52.70.-m, 52.80.-s

I. INTRODUCTION

The electron temperature (T_e) is arguably the most important parameter for low-pressure, high-density plasmas used in microelectronics manufacturing. It governs the rates of ionization, dissociation, and excitation processes in the plasmas. It also determines potentials, and therefore fluxes and energies of charged particles. Much effort has been spent to create plasmas with lower T_e to minimize etching profile anomalies such as “notching” (horizontal attack of polycrystalline-Si (poly-Si) at the interface with the underlying SiO₂ layer) and to reduce plasma-induced device damage due to charge buildup [1–4]. With typical electron temperatures between 1 and 3 eV, a change in T_e as small as 0.2 eV can result in significant changes in plasma-induced potentials across the wafer and can make the difference between damaging and damage-free processes [5]. Therefore, the precise measurement and monitoring of T_e is a continuing concern in plasma studies as well as in plasma-aided manufacturing.

The traditional tool for measuring T_e is the Langmuir probe [6]. Despite an apparent ease of implementation, however, the Langmuir probe technique requires a return circuit, and has to deal with low- and high-frequency plasma potential fluctuations, magnetic fields, and insulating layers [7–9]. It cannot easily be used in depositing environments and, being intrusive, is often a concern for reactor contamination. Thomson scattering, a technique that is routinely used in plasma fusion research to measure T_e , has recently been applied to processing plasma [10]. These measurements were extremely difficult, however, because of the relatively low electron densities and, hence, very low signals. The complex

experimental setup required for Thomson scattering measurements is also not practical for most processing applications.

Among the many optical diagnostic techniques for plasmas, the spectroscopy of emission induced by the plasma is the most widespread method, due to its nonintrusiveness and ease of implementation. In processing plasmas, there have been several attempts to use optical emission spectroscopy (OES) to measure T_e or the electron energy distribution function (EEDF) [11–15]. The general approach is to compare relative emission intensities that are excited by electrons from different parts of the EEDF. These intensities are signatures of the population of emitting levels by electron impact excitations, and their rates are the convolutions of the EEDF and the corresponding cross sections. Typically, two emission lines are observed, and the EEDF is assumed to be a Maxwellian, such that the electron energy probability function (EEDF) is a straight line on a logarithmic scale vs electron energy. T_e is obtained from the inverse slope of this plot. T_e in the model is varied until the ratio of the two computed intensities becomes equal to the ratio of the observed intensities. In cases when both emission lines are from neutral states with similar energies and are therefore excited by electrons from similar parts of the EEDF, the error in T_e measured by this method can be large because of the uncertainties in the cross sections. A comparison of atomic and ionic emission intensities can eliminate this problem if ionic emission is excited in a single, high-energy electron collision with the neutral, but this assumes a Maxwellian distribution over a *very large* range of the EEDF. If instead ionic emission is excited by electron impact excita-

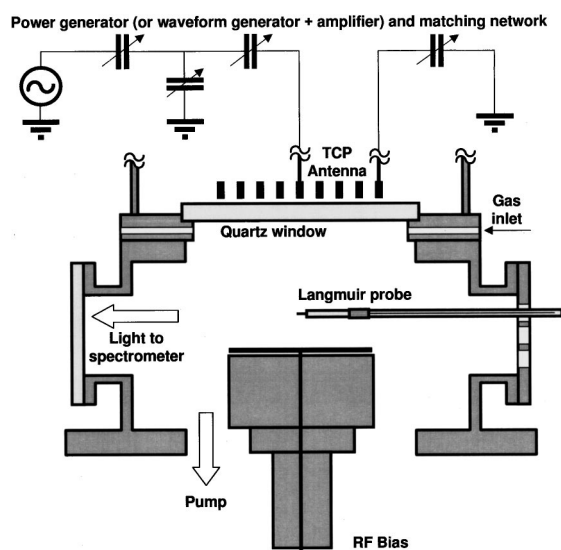


FIG. 1. Schematic representation of the laboratory transformer-coupled plasma (TCP) reactor, radio frequency power matching network, and Langmuir probe and geometry for optical emission spectroscopy. The drawing is to scale; the coil diameter is 15.2 cm.

tion of the ions, then a determination of the absolute ion density is required.

Recently, we reported a nonintrusive method to measure electron temperature—trace rare gases optical emission spectroscopy (TRG-OES) [16] that is more precise and robust than the two-line OES techniques. In this method a small amount ($\sim 5\%$ of total feed gas) of five rare gases (He, Ne, Ar, Kr, and Xe) is added to the plasma, and from the relative intensities of about 20 atomic lines, T_e is determined by comparing the experimental and calculated intensities. The population of the emitting states is modeled by electron impact excitation from both the ground state and through metastable levels that are shown to be very important. These atomic lines have thresholds of excitation from the ground state between 9 and 15 eV and effective excitation energies between 8 and 18 eV, ensuring high precision and sensitivity of the method. (The effective excitation energy can be lower than the threshold energy due to two-step excitation processes through the metastable levels.) The small amount of the added inert gas mixture does not perturb the plasma. Unlike the Langmuir probe method, it is essentially nonintrusive, portable, and applicable to any (e.g., corrosive or depositing) plasma environment.

We have presented electron temperatures obtained by this technique in many different plasmas [5,17–19]. In this study, we describe in detail the TRG-OES method, improve on the model for determining the density of metastable particles, account for gas transport effects on the relative number densities of the rare gases, and discuss the accuracy, precision, and possible limitations of TRG-OES. We also compare previously unpublished TRG-OES and Langmuir probe measurements of T_e in a Cl_2 transformer-coupled plasma (TCP) system.

II. EXPERIMENTAL PROCEDURE

The laboratory transformer-coupled plasma reactor (schematically shown in Fig. 1) consists of stainless steel chamber

(37 cm inner diameter), a He-cooled chuck equipped to hold 5-in.-diam wafers, and a 6-in.-i.d. flat-coil TCP-type antenna positioned just above the quartz window. The coil was powered through an impedance matching network by a 3 kW, fixed frequency (13.56 MHz), radio frequency (rf) generator (Plasma-Therm). The TCP power was varied between 100 and 1000 W. The chuck could be rf biased, but in these experiments was electrically floating at a close to zero (within 1 V) potential. The distance between the chuck and quartz window is adjustable through the vertical motion of the chuck and for these experiments was 15 cm. A mixture of rare gases (1% of each He, Ne, Ar, Kr, and Xe) was added to the Cl_2 plasma. T_e was measured by TRG-OES, as well as with a Langmuir probe.

A spectroscopic system consisting of a 0.64 m focal length monochromator (ISA model HR640) and GaAs photomultiplier tube (Hamamatsu model R943-02) was used to monitor optical emission from the plasma and measure emission intensities of rare gases lines. The spectral resolution was $\sim 0.7 \text{ \AA}$ (with the slits of monochromator set to 100 μm). Line-integrated emission from a $\sim 1\text{-cm}$ -diam cylinder, $\sim 2 \text{ cm}$ above the wafer, was imaged onto the spectrometer entrance slit with fused silica lenses. The relative response of the monochromator detector was determined using a tungsten filament standard lamp.

A single, cylindrical, rf-compensated Langmuir probe (Scientific Systems, Ltd. Smart Probe) was used to obtain current-voltage characteristics (I - V curves) of the plasma. The probe was equipped with a reference electrode to monitor and correct for shifts and low-frequency oscillations in the plasma potential. T_e was determined from the exponential part of the electron retardation region of the I - V curves, as described previously [9,20]. Because the chamber walls were stainless steel, they provided an excellent grounded surface for stabilizing the plasma potential by supplying electrons to the plasma during positive voltage sweeps on the single Langmuir probe. This also allowed the probe to be efficiently cleaned by periodically drawing large electron currents to heat the probe tip. Consequently, T_e and electron densities determined from the Langmuir probe in this study are more accurate and reproducible than those obtained in commercial systems with insulating walls [9].

III. DETERMINING T_e FROM TRG-OES

A. General considerations

The emission spectrum from a 1 mTorr Cl_2 plasma at 700 W input power is shown in Fig. 2. The emission from the plasma is dominated by atomic chlorine lines, many of which are off scale. Under these conditions, the strongest of all rare gas emissions is the Xe 8819 \AA line, with the peak intensity of ~ 1.1 . Other sample lines for Ar, Kr, and Xe are denoted in Fig. 2. Figure 3(a) is an expansion of the region near 7640 \AA , showing a portion of the same spectrum containing emission lines from Ar and Xe. Figure 3(b) shows this same region at 20 mTorr. As the pressure increases, the intensity of the Ar line decreases relative to that of the Xe line. Since the emission from Ar is excited by higher-energy electrons, the decrease in the Ar-to-Xe emission ratio reflects the fact that T_e is lower at 20 mTorr than at 1 mTorr. This example illustrates the TRG-OES method.

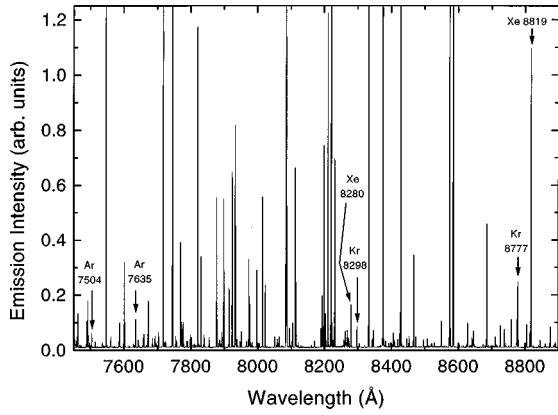


FIG. 2. An emission spectrum from a 1 mTorr Cl_2 plasma at 700 W TCP power. Many of the strong Cl emission lines are off scale.

We determine the electron temperature by adding trace amounts of rare gases (He, Ne, Ar, Kr, and Xe) to the discharge and comparing observed atomic emission intensities with those computed from a model with T_e as an adjustable parameter. Typically, there is no detectable emission from Ne or He (excitation energies >18 or >21 eV) in Cl_2 plasmas. In cases where T_e is higher, such as argon or oxygen plasmas, weak Ne emission is detectable, and further information can be obtained about the EEDF at higher electron energies [21].

The procedure for extracting T_e from the rare gases emission intensities was described previously [16]. Here we review this procedure and further expand upon it to provide a better treatment of the contribution of metastables. We also describe a better method for evaluating the goodness of the model fit.

We record emissions from the Paschen $2p_x$ ($x=1-10$) levels of Ar, Kr, and Xe (see, for example, the atomic energy level diagram for Ar in Fig. 4) as they decay to one of the four $1s$ states. We adopt the subscripts g for the ground state, x for the $2p_x$ states, m for the $1s_3$ or $1s_5$ metastable states, r

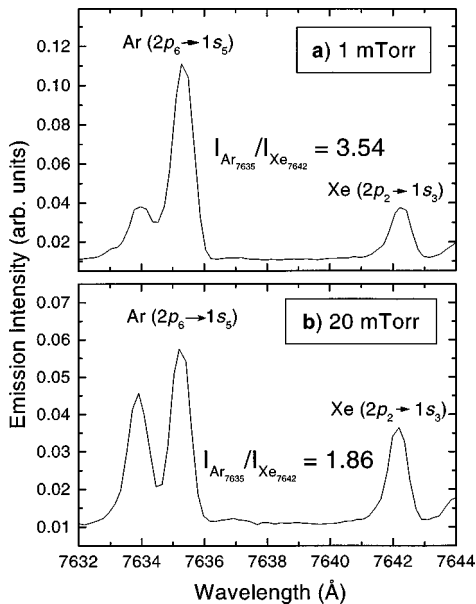


FIG. 3. Partial spectra of Cl_2 plasmas at 700 W TCP power and pressures of (a) 1 mTorr and (b) 20 mTorr.

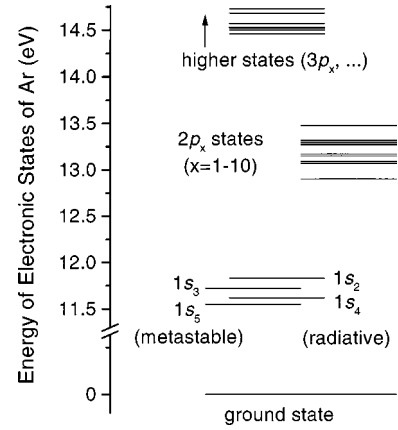
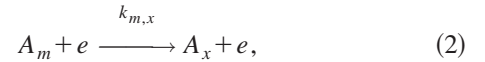
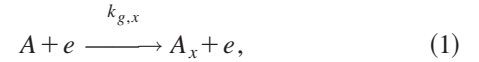


FIG. 4. Energy level diagram of Ar.

for the $1s_2$ or $1s_4$ low-lying radiative states, and s for any $1s$ state. Emitting $2p_x$ levels of the rare gas A can be populated through electron impact excitation from the ground state [Eq. (1)] or the metastable states [Eq. (2)]:



or through radiative decay from the higher states that are initially excited by electron impact. This latter effect is called cascading and can be both pressure independent and pressure dependent [22]. Pressure-independent cascading is included implicitly in processes (1) and (2) where the appropriate apparent cross sections that include collision-free cascading are used (instead of the direct cross sections) to derive the apparent electron impact excitation rate coefficients $k_{g,x}$ and $k_{m,x}$. The pressure-dependent part of cascading can be neglected under low-pressure conditions used here and, in general, at rare gas partial pressures <0.5 mTorr [22]. Likewise, radiation trapping of $2p_x \rightarrow 1s$ emission can be ignored because of the low $1s$ level populations at these low partial pressures.

The observed emission intensity ($I_{A_{x,s}}$) of the transition $A_x \rightarrow A_s$ at wavelength $\lambda_{x,s}$ is therefore given by [23]

$$\begin{aligned} I_{A_{x,s}} &= \alpha(\lambda_{x,s}) Q_x b_{x,s} (n_{A_g} k_{g,x} + n_{A_m} k_{m,x}) \\ &= \alpha(\lambda_{x,s}) Q_x b_{x,s} \sum_{k=g,m} n_{A_k} 4\pi \int_{v_{0,A_{x,k}}}^{\infty} \sigma_{A_{x,k}}(v) v^3 f_e(v) dv, \end{aligned} \quad (3)$$

where $\alpha(\lambda_{x,s})$ is the spectrometer sensitivity at $\lambda_{x,s}$, $\sigma_{A_{x,k}}(v)$ is the cross section at electron speed v for electron impact excitation of level A_x from A_k [$\sigma_{A_{x,k}}(v)=0$ for $v < v_{0,A_{x,k}}$], and n_{A_g} and n_{A_m} are ground-state and metastable-state number densities. The cross sections used for reaction (1) are those of Lin and co-workers [22, 24] for Ar and Xe, and those of Feltsan and Zapesochny [25] for Kr. These data, modified by small correction factors for the Kr values are summarized elsewhere [20,26]. For reaction (2), we used cross sections measured by Boffard *et al.* [27] where avail-

able (for Ar) and by Mitureva, Penkin, and Smirnov [28,29] for Kr and Xe, scaled for better agreement with related pulsed plasma measurements [26] and Born-Bethe calculations by Winstead and McCoy [30]. The number density of metastable particles (n_{A_m}) is a function of n_{A_g} , n_e , and T_e , species concentrations and reactor dimensions, and is discussed below. The ground-state number densities cannot simply be obtained from the input flow rates for the rare gases. The number density for each rare gas is instead a function of its pumping speed by the turbomolecular pump, and its conductance in the tube and through the valve connecting the pump to the plasma chamber. This important effect is treated in detail in the Appendix. It is shown in the appendix that Ar is transported at an efficiency of 1.6 times that of Xe. Consequently, emission from Ar is suppressed by that factor relative to Xe. All electron temperatures presented below are corrected by factors computed from the procedure given in the Appendix. If such effects are ignored, T_e may be underestimated by up to $\sim 30\%$.

For emission of a photon by an atom, the quantum yield Q_x when A_x spontaneously relaxes to any lower state is given by

$$Q_x = \frac{\tau^{-1}}{\tau^{-1} + k_q P}, \quad (4)$$

where τ and k_q are the radiative lifetime and effective quenching rate coefficient for A_x by all species at total pressure P . For the short radiative lifetimes of the emitting states (e.g., for the Ar $2p_1$ level, $\tau = 21$ ns) and at the low pressure used in this study, $Q_x = 1$. Therefore, since every populated level is destroyed by radiative decay only, the rate of population in the model can be directly translated into emission intensity. In Eq. (3), $b_{x,s}$ is the branching ratio for the transition $A_x \rightarrow A_s$, defined as

$$b_{x,s} = \frac{i_{A_{x,s}}}{\sum_{j=1} i_{A_{x,j}}}, \quad (5)$$

where $i_{A_{x,s}}$ is the relative intensity (photons/s) of emissions from level A_x to level A_s , determined from these or other experiments or derived from quantum mechanics, and the summation in the denominator represents allowed transitions from A_x to all lower $1s$ levels, determined in the same manner.

If an electron velocity distribution function $f_e(v)$ can be approximated (at least over the range of $10 < E < 20$ eV) by a Maxwellian with an electron temperature T_e ,

$$f_e(v) = n_e \left(\frac{m_e}{2\pi k T_e} \right)^{3/2} \exp\left(-\frac{m_e v^2}{2k T_e} \right), \quad (6)$$

and if all of the other parameters in Eq. (3) are known, then the relative emission intensities can be compared with ones computed from the model, with T_e as the only adjustable parameter. In principle, a comparison of experimental and modeled intensities for just two emission lines can provide T_e . It is necessary, however, to use as many emission lines as possible to compensate for errors in the electron impact

excitation data, increase the robustness of the method, and possibly obtain an approximate EEDF.

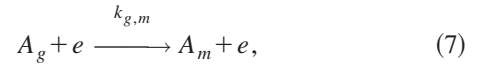
B. Concentration of the metastable particles

1. Creation and loss processes for metastables

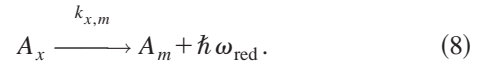
Since only the relative values of emission intensities are important in the model, we can express the densities of atoms in different excited states as a fraction of atom density in the ground state (n_{A_g}). As will be clear from the analysis below, n_{A_g} is always much higher than a sum of atom densities in all excited states and, therefore, can be assumed to be given by the procedure described in the Appendix.

The total emission intensity ($I_{A_{p,s}}$) in Eq. (3) is determined by summing over the electron impact excitation processes from all lower states. For Ne, Ar, Kr, and Xe, these are the ground state (1S_0) and the metastable states $1s_3$ and $1s_5$ (3P_0 and 3P_2). The other two low-lying states $1s_2$ and $1s_4$ (1P_1 and 3P_1) have radiative lifetimes that are short enough [from ~ 3 ns for Xe(1P_1) to ~ 30 ns for Ne(3P_1)] [31] to suppress their steady-state number densities, so excitation out of these states can be ignored.

The metastable states are created by electron impact excitation from the ground state



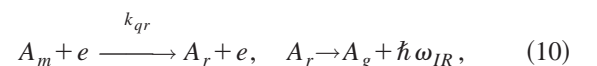
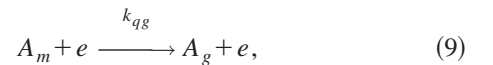
or by radiative decay from higher-energy emitting states

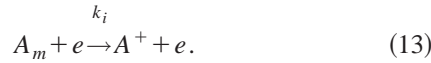
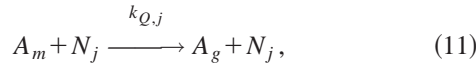


In reaction (8), we include only the emission from the Paschen $2p_x$ levels that are populated by reactions (1) and (2), and neglect direct population of metastable states by optical cascading from levels above $2p_x$, since these states are populated less efficiently than the $2p_x$ levels and, if excited, tend to decay into $2p_x$ states rather than metastables [22, 24].

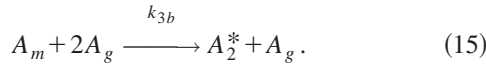
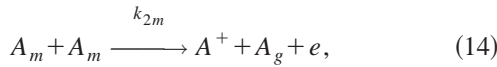
Since, as discussed above, an atom decays spontaneously from the $2p_x$ levels to either metastable ($1s_3$ or $1s_5$) or radiative ($1s_2$ or $1s_4$) states with almost 100% probability ($Q_p \approx 1$), the rate coefficient ($k_{x,m}$) for radiative population of a metastable state in Eq. (8) equals the sum of the coefficients for production of that higher emitting level times the branching ratio ($b_{x,m}$) of decay into the metastable state to the total radiative decay of $2p_x$ level [i.e., $k_{x,m} = b_{x,m}(k_{g,x} + k_{m,x})$].

The metastable states are destroyed by the electron impact excitation [Eq. (2)], electron collisional deexcitation to the ground state [Eq. (9)], electron collisional transitions to $1s_2$ and $1s_4$ states with a subsequent radiative decay to the ground state [Eq. (10)], quenching by collisions with neutral species j (includes Penning ionization) [Eq. (11)], diffusion-controlled quenching of metastable particle at the walls [Eq. (12)], and electron impact ionization [Eq. (13)]:





Similar (or simplified) calculations of Ar metastables number densities (treating 3P_2 and 3P_0 levels as a sum) in Ar plasmas were conducted by several groups [32–35]. The most complete model by Karoulina and Lebede [32] includes reactions (7)–(13), but also considers metastable-metastable [Eq. (14)] and three-body collision [Eq. (15)] quenching:



However, even at the relatively high pressure of ~ 1 Torr in their study (and therefore relatively high concentration of metastable particles with respect to the electron density) the contributions from reactions (14) and (15) were small. In our case, the contributions from these reactions to the destruction of the metastables at all conditions are less than 0.5% and can be neglected.

We compute the density of both metastable levels ($n_{A_{1s5}}, n_{A_{1s3}}$), the sum of which equals n_{A_m} . This is important for computing the emission intensities from $2p_x$ levels that are largely populated through the metastable route, especially in cases where the cross section for electron impact excitation from one of the metastable levels is much larger than that from the other. The same destruction rate is assumed for both levels since these rates are similar, or are measured for only one level or for a mixture with unknown fractions of the two levels. Since the excitation rates into the two levels are different and relatively well measured, however, we keep track of their separate densities. Thus, the ratio of the density of metastable levels corresponds to the ratio of the rates of electron impact excitation into $1s_5$ and $1s_3$ levels, and typically is $n_{A_{1s5}}/n_{A_{1s3}} \sim 5/1$. The cross section for electron impact excitation to level $2p_x$ from the metastable levels is then expressed as

$$\sigma_{A_{m,x}} = \frac{n_{A_{1s5}}}{n_{A_{1s5}} + n_{A_{1s3}}} \sigma_{A_{1s5,x}} + \frac{n_{A_{1s3}}}{n_{A_{1s5}} + n_{A_{1s3}}} \sigma_{A_{1s3,x}}, \quad (16)$$

where $n_{A_{1s5}} + n_{A_{1s3}} = n_{A_m}$.

Solving for the steady state of reactions (7)–(13), we obtain the number density of metastables:

$$n_{A_m} = \frac{n_A \left[k_{g,m} + \sum_{x=1}^{10} k_{g,x} b_{x,m} \right]}{\sum_{x=1}^{10} k_{m,x} (1 - b_{x,m}) + k_{qe} + k_i + \frac{1}{n_e} \left[\sum_j k_{Q,j} n_{N_j} + k_d \right]}, \quad (17)$$

where k_{qe} is a sum of k_{qg} and k_{qr} ; $k_{Q,j}$ and $n_{N,j}$ are the quenching rate coefficient and the density of neutral species N_j . The rate coefficients for formation of the metastable states out of the ground state are computed from

$$k_m = 4\pi \int_0^\infty \sigma_{A_{g,m}}(v) v^3 f_e(v) dv, \quad (18)$$

where $\sigma_{A_{g,m}}(v)$ is the cross section at electron speed v for electron impact excitation of metastable level A_m from the ground state.

Published cross sections or the reaction rate coefficients for reactions (7) and (9)–(12) have been previously reviewed [16]. To calculate rate coefficients for reaction (13), we used cross sections given by McGuire [36]. Diffusion of A_m in the Cl/Cl₂ gas can be approximated as a first-order process, with a rate coefficient of [23]

$$k_d = D_{A_m N_j} / l_{\text{eff}}^2, \quad (19)$$

where l_{eff} is an effective length in the plasma, which is approximately the reactor volume-to-surface area ratio. The effective diffusion coefficient $D_{A_m N_j}$ needed to calculate the rate of diffusion of metastable rare gas atoms in the carrier gas [reaction (12)] can be expressed as

$$D_{A_m N_j} = \frac{1}{1/D_{A_m}^0 + 1/D_{A_m N_j}^p}, \quad (20)$$

combining a molecular diffusion coefficient ($D_{A_m}^0$)

$$D_{A_m}^0 = \frac{l_{\text{eff}}}{3} \sqrt{\frac{8RT_g}{\pi M_A}}, \quad (21)$$

and a pressure-dependent binary diffusion coefficient ($D_{A_m N_j}^p$). T_g is the gas temperature and M_A is the atomic weight of A . $D_{A_m N_j}^p$ was calculated using Lennard-Jones potentials [37], summarized in an earlier version of the TRG-OES model [16], and in a recent study involving diffusion of Cl atoms in a Cl/Cl₂ mixture plasma [38].

We did not measure the gas temperature in this study. From other published studies in similar systems, we assumed a T_g of 300 K (the wall temperature, T_w) at very low TCP power and 1000 K at a power of 1000 W. T_g was assumed to be a linear function of power between these limits. The gas number density was assumed to decrease in proportion to increasing T_g . The total number density was assumed to increase with increasing percent dissociation (%d) of Cl₂. Combining dissociation and heating effects, the total number density (ignoring the rare gases) is given by

$$n_g = \left(\frac{T_g}{T_w} \right) \left(n_{\text{Cl}_2}^0 \left[\frac{100 + \beta \% \text{d}}{100} \right] \right), \quad (22)$$

where $\beta \approx 0.7$ is a correction factor for mass balance that arises from the difference in pumping speeds of Cl and Cl₂ (see the Appendix).

As an example, we present (Table I) calculated rates for population and depopulation of metastable states of Ar, Kr, and Xe in a 10 mTorr Cl₂ plasma at 430 W input TCP power. Under these conditions, $n_e = 1 \times 10^{11} \text{ cm}^{-3}$ and 74% of the Cl₂ is dissociated [39]. The columns in Table I represent

TABLE I. First-order reaction rate coefficients for excitation and deexcitation of metastable states Ar, Kr, and Xe (10 mTorr, 74% dissociated Cl₂ plasma; $n_e = 1 \times 10^{11} \text{ cm}^{-3}$, $T_e = 2 \text{ eV}$, $T_g = 600 \text{ K}$, $l_{\text{eff}} = 4 \text{ cm}$).

| | $n_e k_{g,m}$ | $n_e \sum_{x=1}^{10} k_{g,x} b_{x,m}$ | $n_e \sum_{x=1}^{10} k_{m,x} (1 - b_{x,m})$ | $n_e k_{qe}$ | $n_e k_i$ | $\sum_j k_{Q,j} n_{N_j}$ | k_d |
|----|---------------|---------------------------------------|---|--------------------|--------------------|--------------------------|--------------------|
| Ar | 1.87 | 1.03 | 8.13×10^3 | 2.00×10^4 | 1.69×10^3 | 3.62×10^4 | 8.43×10^2 |
| Kr | 5.73 | 4.57 | 2.65×10^3 | 1.80×10^4 | 1.29×10^3 | 3.62×10^4 | 6.61×10^2 |
| Xe | 29.87 | 6.15 | 8.66×10^3 | 1.50×10^4 | 1.69×10^3 | 3.62×10^4 | 4.99×10^2 |

first-order rates of, respectively, excitation from the ground state to the metastable states, population from $2p_x$ states excited from the ground state, depopulation through excitation out of the metastable states into $2p_x$ states with subsequent decay into the radiative states, electron quenching to the ground states or radiative states, electron impact ionization, quenching by molecular and atomic (negligible) chlorine, and diffusion.

2. Dependence of the metastable concentration on plasma parameters

Figure 5 presents the calculated densities of Ar, Kr, and Xe metastables, relative to the corresponding ground-state densities as a function of electron temperature for a 10 mTorr Cl₂ plasma in the TCP reactor described in Sec. II. Above, we assumed that the total number density of all excited levels [40] is negligible with respect to the density of the ground state. For the typical range of T_e 's the density of metastables is less than 1% of the ground-state density, so this assumption is valid.

Another key variable in determining the concentration of the metastable particles is electron density. Figure 6 shows number density of Ar metastables as a function of n_e at constant T_e . $n_{m,\text{Ar}}$ is calculated for four different cases with Cl₂ as the feed gas (Cl₂ is one of the most commonly used gases in plasma etching). The left most dashed line corresponds to a Cl plasma (i.e., 100% dissociation of the Cl₂ feed gas) with the traces of rare gases. In this case, the destruction of the metastables by neutral species (Cl and the rare gases) is negligible and $n_{m,\text{Ar}}$ reaches saturation at $n_e = 10^{11} \text{ cm}^{-3}$

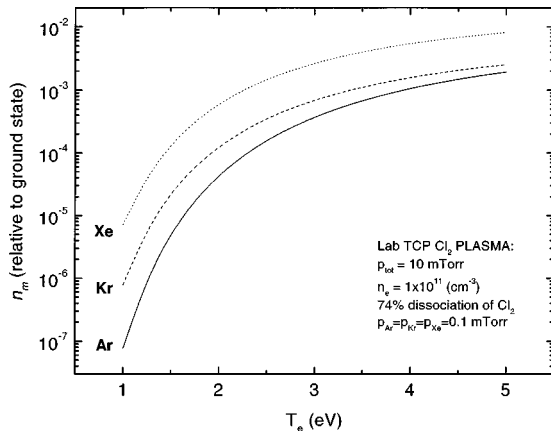


FIG. 5. Computed number densities (relative to the respective ground state) of Ar, Kr, and Xe metastables in the laboratory TCP reactor (Fig. 1) at a Cl₂ pressure of 10 mTorr for the range of T_e , with the other plasma parameters fixed.

[see Eq. (17)]. At the opposite limit, no dissociation of Cl₂ occurs, the metastables are mainly destroyed by collisions with Cl₂, and the metastable density increases from near zero at $n_e = 10^{10} \text{ cm}^{-3}$ to its saturation value at $n_e = 3 \times 10^{15} \text{ cm}^{-3}$ (Fig. 6, the dashed line on the right). The dashed line in the middle corresponds to 74% dissociation (measured at 10 mTorr in the TCP reactor described above at an input power corresponding to $n_e = 1 \times 10^{11} \text{ cm}^{-3}$).

The three dashed curves in Fig. 6 were calculated with a fixed percent dissociation of Cl₂. In practice, when the input power increases, so does the electron density and the percent dissociation [38]. The solid line in Fig. 6 represents the dependence of $n_{m,\text{Ar}}$ on n_e with a measured Cl₂ percent dissociation that increases with increasing n_e . In this case, the metastable density increases from near zero to its saturation value when n_e increases from 10^{10} to 10^{12} cm^{-3} . Over this range of n_e , the derivation of the adjustable parameter T_e from a comparison of computed and observed emission intensities requires knowledge of n_e . Conversely, n_e can be treated as a second adjustable parameter, allowing electron densities in the $\sim 10^{10} - 10^{12} \text{ cm}^{-3}$ to be estimated from the best fit of the model to the data.

C. Procedures to compute T_e from comparisons of observed and computed emission intensities

The use of a large number (~ 25) of emission lines from Ar, Kr, and Xe helps to average out random uncertainties in

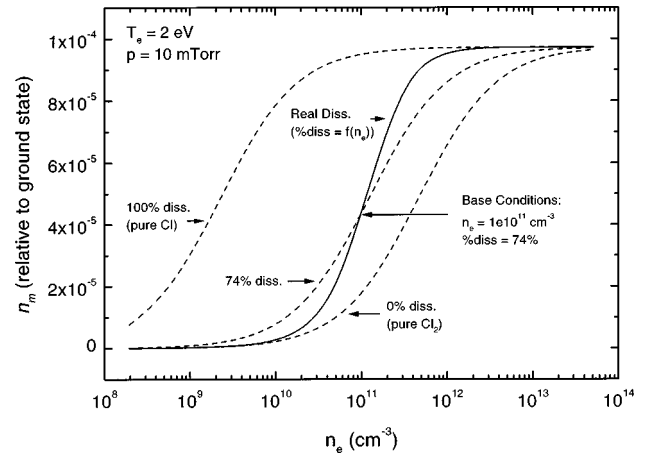


FIG. 6. Computed number densities of Ar metastables ($n_{m,\text{Ar}}$) in the laboratory TCP reactor (Fig. 1) as a function of n_e for $p = 10 \text{ mTorr}$ Cl₂, and $T_e = 2 \text{ eV}$. The assumed values for percent dissociation of Cl₂ are (dashed lines from left to right) 100%, 74% (measured percent dissociation at the input power corresponding to $n_e = 10^{11} \text{ cm}^{-3}$), and 0%. The solid line represents a calculation in which the percent dissociation is also a function of electron density (determined from experiments).

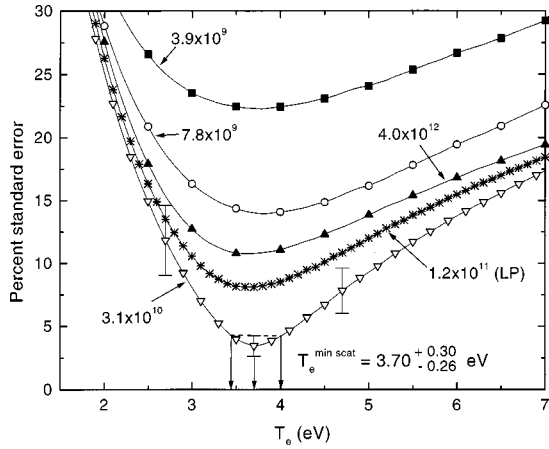


FIG. 7. The “minimum scatter” method for determining T_e from TRG-OES. The percent standard error of the sets of values of $\ln(I_{\lambda,\text{expt}}/I_{\lambda,\text{calc}})$ for all lines is plotted as a function of the input T_e in the model (for several different n_e input values). The experimental intensities are those measured in a 2 mTorr Cl_2 plasma in the laboratory TCP reactor with 500 W input TCP power.

the electron impact excitation cross sections and other sources of random error. The best fit of the model to experimental data is the best match of the *relative* calculated intensities ($I_{\lambda,\text{calc}}$) to the observed experimental intensities ($I_{\lambda,\text{expt}}$) at $\lambda_{x,s}$, i.e., $I_{\lambda,\text{expt}}/I_{\lambda,\text{calc}} = a$ for all the lines, where a is arbitrary constant that is the same for all emission lines. (An absolute calibration of the spectroscopic system is impractical and unnecessary.)

Typically, we calculate sets of $I_{\lambda,\text{expt}}/I_{\lambda,\text{calc}}$, assuming a Maxwellian EEDF for each T_e between 1 and 8 eV with a 0.1 eV step resolution. Two methods are used to select the best of these 70 sets of emission intensity ratios and, therefore, the best value for T_e . In the first method, the weighted mean values (with weights of individual ratios determined by their uncertainties) of $\ln(I_{\lambda,\text{expt}}/I_{\lambda,\text{calc}})$ for all of the lines, together with the percent standard error $\sigma(T_e)$, are calculated for each set. The percent standard error around the mean value is plotted as a function of input T_e for each input n_e (see Fig. 7). The lowest percent standard error (or *minimum scatter*) corresponds to the best match between the model and the experiment and hence the best value for T_e (denoted as $T_e^{\text{min scat}}$ in Fig. 7).

Along with the electron temperature, the model also requires a value for n_e . If available, we use a value from Langmuir probe or microwave interferometry experiments. If such data are not available, we use an educated guess. In both cases, we allow the values of n_e to vary, typically from $n_{e,0}/32$ to $32n_{e,0}$ in increments of a factor of 2. The minimum percent standard deviation (defined as above) is then determined for all the values of n_e , and the set with the lowest scatter for all possible n_e and T_e determines the final T_e value. Such an approach eliminates the need to know the electron density. We refer to this as the *absolute minimum scatter* method. The absolute minimum scatter of the percent standard error (Fig. 7) determines not only T_e , but also n_e . Because of the relatively large uncertainty in the cross sections of excitations out of the metastable states, however, n_e determined in this manner is not as reliable as the value derived for T_e .

From Fig. 7, the absolute minimum scatter of the percent standard error is found at input parameters of $T_e = 3.70$ eV and $n_e = 3.1 \times 10^{10} \text{ cm}^{-3}$. The Langmuir probe data gave $n_e = 1.2 \times 10^{11} \text{ cm}^{-3}$ (in the center of the reactor), which would yield a TRG-OES T_e of 3.64 eV. Some of the discrepancy between these two values for n_e is attributed to the fact that the Langmuir probe measured the peak n_e in the center of the plasma, while n_e estimated by TRG-OES is a weighted (by emission intensity) line-integrated electron density that includes regions of lower electron density near the walls. The discrepancy could also mean that the model overestimated the contributions from metastables in this example. Since n_e is introduced in the model only through the calculation of metastable densities and contributions to optical emission [see Eq. (19)], it can be allowed to change, compensating for errors in the metastable cross sections. For example, if the contribution from the metastables were overestimated because their cross sections for electron impact excitation were too high, then the best fit in the model would be found with an artificially low n_e . We can see from Fig. 7 that in this particular case, a reasonable guess for n_e is sufficient for determining T_e , since the minimum scatter is obtained at $T_e = 3.7$ eV, independent of assumed electron densities between an extremely low value of $3.9 \times 10^9 \text{ cm}^{-3}$ and a much too high n_e of $4.0 \times 10^{12} \text{ cm}^{-3}$. In other cases, some dependence (usually an increase of never more than 20%) of the minimum scatter T_e was found over this very large range of n_e .

To estimate the absolute uncertainty of T_e from this method, we calculate the uncertainty of the percent standard error of scatter $\Delta\sigma(T_e)$ from combined experimental (important for weak lines that have poor signal to noise ratios) and theoretical (dominated by a 15–45 % uncertainty in the cross section data) uncertainties, using standard propagation of error methods. Sample uncertainties of the percent standard error are shown in Fig. 7 for points at $T_e = 2.7, 3.7,$ and 4.7 eV for $n_e = 3.1 \times 10^{10} \text{ cm}^{-3}$. The lower (T_e^{low}) and upper (T_e^{high}) boundaries for the T_e value obtained in the minimum scatter method are determined from the equation

$$\sigma(T_e^{\text{low}}) = \sigma(T_e^{\text{min scat}}) + \Delta\sigma(T_e^{\text{min scat}}) = \sigma(T_e^{\text{high}}). \quad (23)$$

From the lowest curve in Fig. 7, $\sigma(T_e^{\text{low}})$ and $\sigma(T_e^{\text{high}})$ each define a solution of [Eq. (23)], at $T_e^{\text{low}} = 3.44$ eV and $T_e^{\text{high}} = 4.00$ eV: therefore, $T_e^{\text{min scat}} = 3.70 (+0.30/-0.26)$ eV.

In a second method for determining T_e , the values of $\ln(I_{\lambda,\text{expt}}/I_{\lambda,\text{calc}})$ are plotted vs threshold energy ($E_{\lambda,\text{th}}$) for excitation from the ground state to each of the $2p_x$ level emitting at $\lambda_{x,s}$ for each set, corresponding to the different assumed values of T_e . A linear least-squares fit is then applied to the weighted data of each set, and the slopes (and their uncertainties) of the linear fit are determined (Fig. 8). If T_e in the TRG-OES model is too low, the calculated emission intensities for the lines that are excited mostly by high-energy electrons (Ar lines) are underestimated and the $\ln(I_{\lambda,\text{expt}}/I_{\lambda,\text{calc}})$ values for these lines are too high, while the calculated emission intensities for the lines with the lower threshold energies (Xe) are relatively overestimated. The slope of the linear fit to the $\ln(I_{\lambda,\text{expt}}/I_{\lambda,\text{calc}})$ vs $E_{\lambda,\text{th}}$ points in this case is positive. If instead a too-high T_e is chosen, the

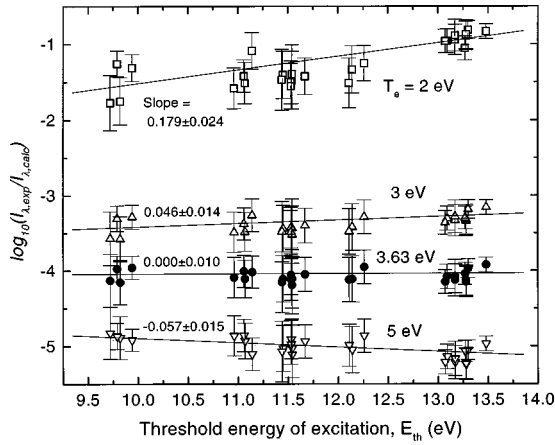


FIG. 8. The “zero slope” method for determining T_e from TRG-OES. $\ln(I_{\lambda,\text{expt}}/I_{\lambda,\text{calc}})$ is plotted vs threshold energies for excitations (for several different T_e input values and a fixed value for n_e determined from Langmuir probe measurements). Experimental intensities are the same as in Fig. 7.

slope is negative. T_e is determined from the set with a slope equal to zero. The uncertainty in T_e is obtained from the standard deviation in the slope of the least-squares-fitted line, and the boundary T_e 's that would provide zero slope within that uncertainty. For example, in Fig. 8 this *zero-slope* method yields $T_e = 3.63$ eV, in excellent agreement with the minimum scatter value of 3.70 eV in Fig. 7. This second method does not have the capability of determining electron density and requires a value for n_e as an external parameter. As with the minimum scatter methods, the value for n_e can be an educated guess, or a measurement provided by Langmuir probe or microwave interferometry analysis. It can also be the value of n_e determined from the absolute minimum scatter method.

The agreement between the absolute minimum scatter and zero-slope methods is typically very good (\sim few percent). The final value provided by TRG-OES is a weighted average between the minimum standard error and the zero-slope method. (In the example of a 2 mTorr Cl_2 plasma at 500 W power, the weighted average and combined uncertainties yield $T_e = 3.68 \pm 0.24$ eV).

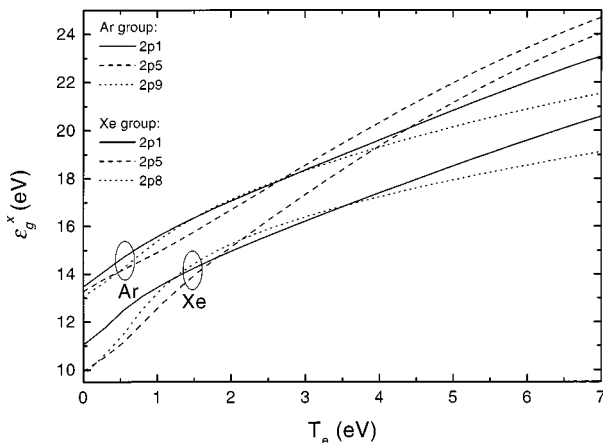


FIG. 9. Effective energies (defined in text) for excitations from the ground state of several Ar and Xe lines as functions of T_e .

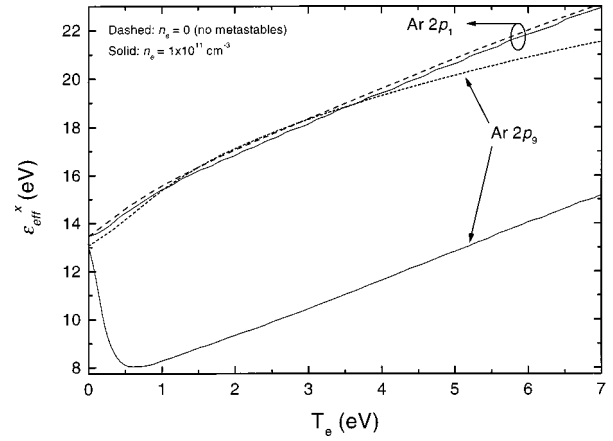


FIG. 10. Effective energy of excitation of Ar $2p_1$ and $2p_9$ levels as functions of T_e . Dashed lines, metastables not included (as in Fig. 9): solid lines, metastables included ($n_e = 1 \times 10^{11} \text{ cm}^{-3}$, 10 mTorr Cl_2 , 74% dissociation).

D. Sensitivity of TRG-OES to the EEDF

The energies of the emitting $2p$ Paschen states of rare gases used in the method are between 9.72 eV ($2p_8$ level of Xe) and 13.48 eV ($2p_1$ level of Ar). Consequently, one would expect the TRG-OES method to be sensitive to the high energy part of the EEDF, since only electrons with energies higher than these thresholds can populate these levels from the ground state. Let us define the “effective” energy of an “average” electron that is responsible for the excitation of the emitting level x out of the ground state:

$$\epsilon_{\text{eff}}^{g,x}(T_e) \equiv \frac{\langle \epsilon v \sigma_{g,x}(\epsilon) \rangle}{\langle v \sigma_{g,x}(\epsilon) \rangle} = \frac{\int_0^\infty \epsilon \sqrt{\frac{2\epsilon}{m_e}} \sigma_{g,x}(\epsilon) f(\epsilon) d\epsilon}{\int_0^\infty \sqrt{\frac{2\epsilon}{m_e}} \sigma_{g,x}(\epsilon) f(\epsilon) d\epsilon}, \quad (24)$$

where ϵ and $f(\epsilon)$ are the electron energy and electron energy distribution function. Since $f(\epsilon)$ (which we again, for sim-

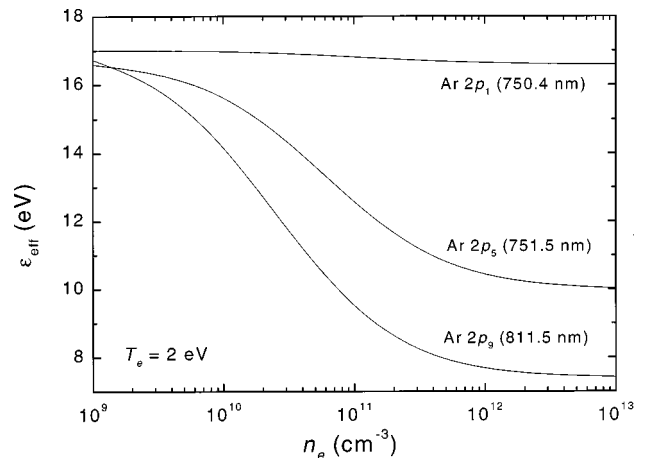


FIG. 11. Dependence of the effective energies of Ar $2p_1$, $2p_5$, and $2p_9$ levels on electron density. $T_e = 2$ eV, 10 mTorr Cl_2 , 74% dissociation.

plicity, assume to be Maxwellian) is a function of T_e , the effective electron energy is also a function of T_e .

The effective energies for excitation of Ar $2p_1$, $2p_5$, and $2p_9$ and Xe $2p_3$, $2p_5$, and $2p_8$ levels as functions of T_e are shown in Fig. 9. In the limit of $T_e \rightarrow 0$, these effective energies reduce to the energies of the corresponding levels above the ground state or the threshold energies for excitation. Although the energies of the $2p$ levels are ordered

$$\varepsilon_{2p_{10}}^{\text{Xe}} < \dots < \varepsilon_{2p_1}^{\text{Xe}} < \varepsilon_{2p_{10}}^{\text{Kr}} < \dots < \varepsilon_{2p_1}^{\text{Kr}} < \varepsilon_{2p_{10}}^{\text{Ar}} < \dots < \varepsilon_{2p_1}^{\text{Ar}}, \quad (25)$$

one can see from Fig. 9 that the order of $\varepsilon_{\text{eff}}^{g,x}$ may change at T_e different from $T_e \rightarrow 0$.

As discussed above, the excitation of an emitting $2p$ level can occur through electron impact excitation of one of the metastable levels that are also formed by electron impact (from the ground state). Such two-electron transitions have lower excitation thresholds and can be caused by lower-energy electrons than excitations directly from the ground state. To take the excitation out of the metastables into account, we can define the effective energy for the excitation of $2p_x$ level as

$$\begin{aligned} \varepsilon_{\text{eff}}^x(T_e, n_e) &\equiv \frac{\langle \varepsilon v \sigma_{g,x}(\varepsilon) \rangle + n_m \langle \varepsilon v \sigma_{m,x}(\varepsilon) \rangle}{\langle v \sigma_{g,x}(\varepsilon) \rangle + n_m \langle v \sigma_{m,x}(\varepsilon) \rangle} \\ &= \frac{\int_0^\infty \varepsilon \sqrt{\frac{2\varepsilon}{m_e}} \sigma_{g,x}(\varepsilon) f(\varepsilon) d\varepsilon + n_m \int_0^\infty \varepsilon \sqrt{\frac{2\varepsilon}{m_e}} \sigma_{m,x}(\varepsilon) f(\varepsilon) d\varepsilon}{\int_0^\infty \sqrt{\frac{2\varepsilon}{m_e}} \sigma_{g,x}(\varepsilon) f(\varepsilon) d\varepsilon + n_m \int_0^\infty \sqrt{\frac{2\varepsilon}{m_e}} \sigma_{m,x}(\varepsilon) f(\varepsilon) d\varepsilon}, \end{aligned} \quad (26)$$

where n_m , as before, is the number density of metastables as a fraction of the ground-state number density. The effective excitation energies decrease with the introduction of the metastables, as shown in Fig. 10. The effective energies for excitation of Ar $2p_1$ (emitting at 750.4 nm) and $2p_9$ (emitting at 811.5 nm) are shown for two conditions: $n_e \rightarrow 0$ (dashed lines, corresponding to absence of metastable levels, as in Fig. 9) and $n_e = 1 \times 10^{11} \text{ cm}^{-3}$ (solid lines, in a 10 mTorr, 74% dissociated Cl_2 plasma).

The effective energy for excitation of emission from the Ar $2p_1$ level is independent of n_e and nearly equal to $\varepsilon_{\text{eff}}^{g,x}$ since the cross section for electron impact excitation of this level from the metastable levels is very small, and therefore the contribution of emission excited from metastable levels to the total emission is negligible. On the other hand, the effective energy of the Ar $2p_9$ level (to which the contribution from excitation out of the metastable levels is substantial) changes significantly. Consequently, while rare gas metastables bring a major complexity to the method, they also greatly increase the range of electron energies contributing to T_e derived from the model. In the example given in Fig. 10, without the metastables, emission from Ar $2p_1$ and $2p_9$ would provide information about essentially the same part of the EEDF (e.g., 14 eV at low T_e and 20 eV at $T_e \sim 5$ eV), while with the metastables they reflect different EEDF regions (a 7 eV spread at $T_e > 0.5$ eV).

Since the number density of metastables is also a function of n_e , the effective energy of excitation decreases with increasing n_e , as more metastables particles are created. Figure 11 illustrates this point for the $2p_1$, $2p_5$, and $2p_9$ Ar levels. In the limit of $n_e \rightarrow 0$, $n_{A_m} \rightarrow 0$ and $\varepsilon_{\text{eff}}^x \rightarrow \varepsilon_{\text{eff}}^{g,x}$. As n_e increases, the $\varepsilon_{\text{eff}}^x$ parameters decrease to asymptotic values at high n_e , when n_{A_m} reaches its upper limit.

Finally, we show the entire range of electron energies that are probed with TRG-OES. Without emission from He or Ne, this range is between the effective energies of excitations of Xe $2p_8$ (881.9 nm) and Ar $2p_1$ (750.4 nm), the levels with the lowest and the highest effective energies, respectively. Figure 12 shows the effective energies of these levels as functions of T_e and n_e . For each set of conditions (T_e, n_e) , the distance between lower (Xe $2p_8$) and upper (Ar $2p_1$) surfaces represent the range of EEDFs probed by TRG-OES. The projection of these surfaces on the $n_e = 0$ plane (no metastables) would provide the curves from Fig. 9. At plasma parameters most relevant to processing, the range of the EEDFs probed by TRG-OES is about 10 eV.

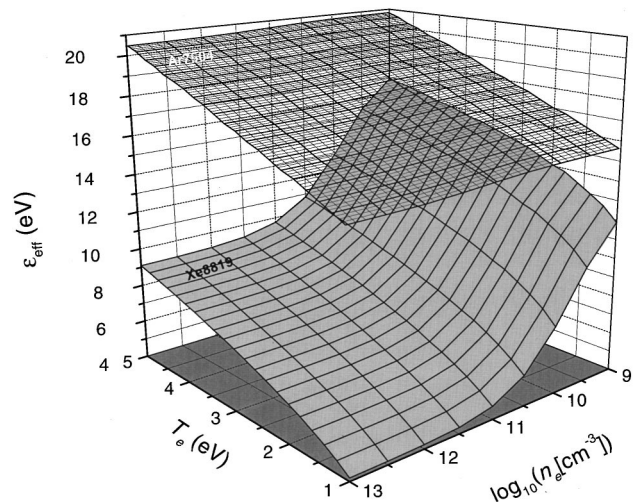


FIG. 12. The effective energies for excitations of Xe $2p_8$ (881.9 nm) level (lower gray surface) and Ar $2p_1$ (750.4 nm) level (higher wire surface) as functions of T_e and n_e in a 10 mTorr, 74% dissociated Cl_2 plasma.

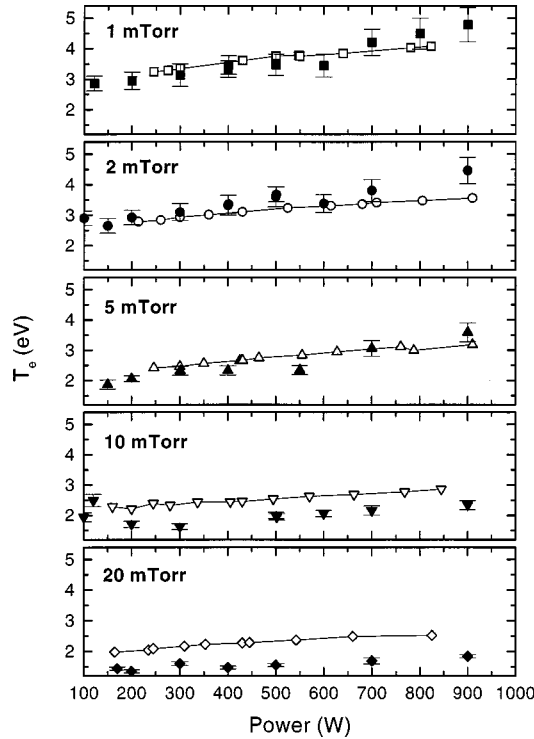


FIG. 13. T_e as a function of TCP power and pressure (1, 2, 5, 10, and 20 mTorr) measured by TRG-OES (solid symbols) and the Langmuir probe (open symbols connected by lines).

IV. RESULTS FROM THE LABORATORY TCP REACTOR

Figure 13 presents electron temperature as a function of power in 95% Cl_2 /5% rare gases plasmas for different total pressures measured both by TRG-OES and the Langmuir probe. Both techniques yield higher values of T_e at lower pressure and higher power, but differ in manners similar to those observed for other inductively coupled plasma reactors operating at 13.56 MHz [5,17,19]. T_e 's obtained from TRG-OES measurements exhibit stronger pressure dependences and are lower than those obtained with the Langmuir probe at higher pressure.

The main reason for the disparity between the two sets of electron temperatures at high pressures is that they sample different regions of a non-Maxwellian EEDF. Figure 14 presents electron energy probability functions at different pressures. As discussed above, TRG-OES assumes a partially Maxwellian EEDF (straight line on the EEPF between ~ 10 and ~ 20 eV). The Langmuir probe analysis also defines T_e for a Maxwellian EEDF by finding the best fit to the exponential part of the electron retardation region of I - V curves ($3 \leq E \leq 13$ eV). The EEPFs measured with the Langmuir probe at 430 W input TCP power show that only the 1 and 2 mTorr discharges have a Maxwellian electron energy distribution. At higher pressures, the distributions increasingly deviate from Maxwellians through a depletion of the high-energy tail. Thus the results in Fig. 14 explain the difference between the T_e measurements in Fig. 13. At 1 and 2 mTorr (nearly completely Maxwellian distributions) both methods yield similar values for T_e within their combined uncertainties (we estimate an uncertainty of the Langmuir probe T_e 's of ~ 10 – 15 %). At higher pressures (≥ 5 mTorr), however, TRG-OES yields lower values for T_e , sensing the depletion

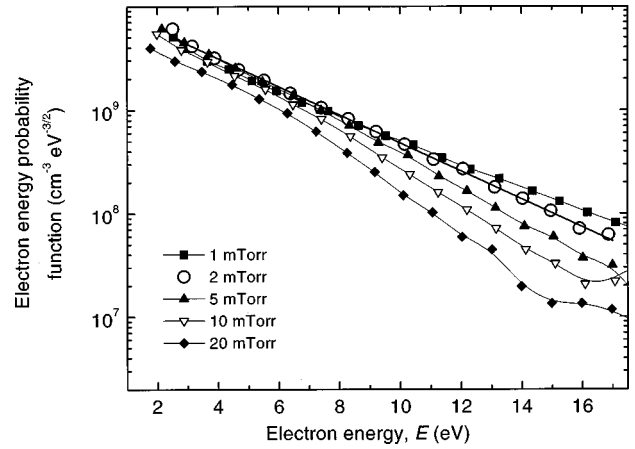


FIG. 14. Electron energy probability functions for 1, 2, 5, 10, and 20 mTorr Cl_2 discharges at 430 W input power, as measured by the Langmuir probe. A straight line (indicating a Maxwellian EEDF) is drawn through the 2 mTorr data.

of the high-energy tail. Also note that the spread in slopes of the high-energy part of the EEPF results in a stronger pressure dependence of T_e from TRG-OES, while a weaker pressure dependence of the Langmuir probe T_e 's reflects the more similar slopes for the bulk of the EEPFs.

V. CONCLUSION

Trace rare gases optical emission spectroscopy is a robust, nonintrusive method to determine electron temperature in low-pressure, high-density processing plasmas. The applicability of the method can be easily extendable to other plasmas, since TRG-OES requires an addition of only a small amount of chemically inert gases and a spectroscopic system with an optical (visible range) access to the plasma. In processing plasmas, TRG-OES is the only (and, in most cases, better) alternative to the Langmuir probe technique, which fails in hostile environments and possesses a number of artifacts. While the Langmuir probe samples mostly bulk and mid-energy electrons, TRG-OES samples mostly the high-energy tail of the EEDF (>10 eV). This is the most important part of the distribution, since these high-energy electrons establish sheaths and potentials across the plasma, provide the electron part of the current to the wafer, and excite, dissociate, and ionize atoms and molecules. With further refining of the rare gas cross sections, particularly those for electron impact excitation of Xe out of the metastable states, and excitation of Kr from both the ground state and metastable states, it should be possible to derive EEDFs from TRG-OES, as well as absolute electron densities.

Comparison of T_e values over a large pressure/power range showed good agreement between TRG-OES and Langmuir probe methods for Maxwellian EEDFs in low-pressure (≤ 5 mTorr) plasmas with well-grounded surfaces (bare stainless steel) exposed to the plasma. The disparity between the two methods at higher pressures (5 mTorr and above) is justified by deviations of the EEDFs from a simple Maxwellian distribution, through a depletion of high-energy electrons.

APPENDIX: CORRECTIONS FOR DIFFERENCES IN RARE GAS PUMPING SPEEDS

The TRG-OES method requires accurate relative number densities for the rare gases. It cannot simply be assumed that

TABLE II. Gas transport parameters, pumping speeds, and correction factors required to correct rare gas number densities their different transport efficiencies.

| Gas | ν (cm s ⁻¹) | S (cm ³ s ⁻¹) | $d(A)$ (Å) | λ (cm, in 1 mTorr Cl ₂) | $\eta(A)$ (10 ⁻⁴ g cm ⁻¹ s ⁻¹) | $n(A)/n(\text{Xe})$ $f(\text{Cl}_2)=20,$ $U=1.65$ | $n(A)/n(\text{Xe})$ $f(\text{Cl}_2)=100,$ $U=26.4$ |
|-----------------|-----------------------------|--|------------|--|--|---|--|
| He | 12.6×10 ⁴ | 1.05×10 ⁶ | 2.18 | 6.54 | 1.98 | 0.405 | 0.241 |
| Ne | 5.61×10 ⁴ | 1.10×10 ⁶ | 2.60 | 5.79 | 3.12 | 0.542 | 0.448 |
| Ar | 3.99×10 ⁴ | 1.02×10 ⁶ | 3.67 | 4.37 | 2.21 | 0.659 | 0.591 |
| Kr | 2.75×10 ⁴ | 8.54×10 ⁵ | 4.15 | 3.90 | 2.50 | 0.853 | 0.824 |
| Xe | 2.19×10 ⁴ | 7.54×10 ⁵ | 4.91 | 3.29 | 2.24 | 1.0 | 1.0 |
| Cl ₂ | 2.99×10 ⁴ | 8.91×10 ⁵ | 5.44 | 2.45 | 1.34 | | |

the number densities are proportional to the flow rates $f(A)$ (and therefore equal in the experiments described above) since the effective pumping speed $S_{\text{eff}}(A)$ is a function of the gas A . The geometry of most plasma reactors can be approximated by a large vessel, connected by a tube of length l_{tube} and diameter d_{tube} to a pump with a pumping speed $S(A)$ that also depends on the gas. Between the pump and vessel is a throttle valve with inner diameter d_{valve} . For the system used in this study, $l_{\text{tube}}=46$ cm, $d_{\text{tube}}=18$ cm, and $d_{\text{valve}}=18$ cm.

The effective pumping speed for the vessel is given by [41]

$$1/S_{\text{eff}}(A) = 1/S(A) + 1/C_{\text{tube}}(A) + 1/C_{\text{valve}}(A), \quad (\text{A1})$$

where $C_{\text{tube}}(A)$ and $C_{\text{valve}}(A)$ are the conductances of the tube and valve. The number density of each rare gas is then

$$n(A) = f(A)/S_{\text{eff}}(A), \quad (\text{A2})$$

where $f(A)$ is the flow rate in (molecules s⁻¹)(1 scm = 4.482×10¹⁷ molecules s⁻¹).

The pumping speed of a turbomolecular pump is a function of the pump's blade geometry and rotation frequency (f), as well as the pressure and mass of the gas. For the lighter gases (He and to a lesser extent Ne), it is also a function of the transmission probability [$k(A)$] and the pressure in the fore line. If the faces of the pump's blades are at a 45° angle with respect to the mean gas flow direction and the spacing between the blades is large compared with the blade thickness, then the low-pressure pumping speed is [41, 42]

$$S(A) = \frac{v_b F}{4[1/k + v_b/\nu(A)]}, \quad (\text{A3})$$

where $\nu(A)$ is the mean thermal speed for A , v_b is the mean blade speed, defined as

$$v_b = \frac{4}{3} \pi f (R_a^3 - R_i^3) / (R_a^2 - R_i^2), \quad (\text{A4})$$

and F is the input area of the disk defined by the outer radius of the blades (R_a) and the inner radius at which the blades merge into a solid hub (R_i):

$$F = \pi(R_a^2 - R_i^2). \quad (\text{A5})$$

For the pump used in this study (Leybold Heraeus model Turbovac 1000C), $f=600$ Hz, $R_a=10.1$ cm, and $R_i=5.1$ cm. Using transmission probabilities of unity [except for the lightest gases: $k(\text{He})=0.69$, $k(\text{Ne})=0.92$] [42], the low-pressure pumping speeds calculated from Eq. (A3) are listed in Table II.

The most important reduced variable considered when estimating tube conductances is the Knudsen number Kn :

$$\text{Kn}(A) = \lambda(A)/d_{\text{tube}}, \quad (\text{A6})$$

where $\lambda(A)$ is the mean free path for a small amount of rare gas A in the process gas. For the gas flow mixture used in this study (1% of each of the rare gases added to 95% Cl₂), the mean free path for the rare gases is given to a good approximation by

$$\lambda(A) = 1/[\sqrt{2} \pi n_g d(A-\text{Cl}_2)^2], \quad (\text{A7})$$

where $d(A-\text{Cl}_2)$ is the diameter of the $A-\text{Cl}_2$ collision pair:

$$d(A-\text{Cl}_2) = [d(A) + d(\text{Cl}_2)]/2. \quad (\text{A8})$$

The degree of Cl₂ dissociation in the plasma is largely irrelevant because (1) Cl recombination is fast on the stainless steel surfaces of the tubing leading to the pump and (2) the mean free path of a rare gas through Cl₂ at a number density n_g is roughly the same as that for the rare gas in Cl at a number density of $2n_g$.

Molecular diameters determined from viscosity data [41] are summarized in Table I. Knudsen numbers for the experiments described above and elsewhere [16,17,19,20,38] range from ~ 0.01 for Xe in Cl₂ at 20 mTorr to ~ 0.5 for Ar in Cl₂ at 0.5 mTorr. Gas flow is molecular for $\text{Kn}(A) > 0.5$, while continuum flow occurs for $\text{Kn}(A) < 0.01$. Therefore, the gas flow just spans the transitional flow regime between these two limits under the conditions typically used in plasma etching processes.

The conductance through an aperture in the transitional flow regime is given by [41]

$$C_{\text{aper}}^t(A) = C_{\text{aper}}^m(A) \left[\frac{10 + k_1 [d_{\text{aper}}/\lambda(A)]^{1.5}}{10 + k_2(A) [d_{\text{aper}}/\lambda(A)]^{1.5}} \right], \quad (\text{A9})$$

where $C_{\text{aper}}^m(A)$ is the aperture conductance for molecular flow, d_{aper} is the smaller dimension of the aperture, $k_1=0.5$, and $k_2(A)$ is given by [41, 43]

$$k_2(A) = \frac{0.5}{\sqrt{2\pi}} \left(\frac{\gamma(A)+1}{2} \right)^{1/(\gamma(A)-1)} \left(\frac{\gamma(A)+1}{2\gamma(A)} \right)^{1/2}, \quad (\text{A10})$$

with $\gamma(A) = C_p(A)/C_v(A)$ being the ratio of constant pressure to constant volume heat capacities (5/3 for atoms and 1.325 for Cl₂ at 300 K [44]). The molecular flow conductance through an aperture is given by [41]

$$C_{\text{aper}}^m(A) = \pi v A_{\text{aper}}/4, \quad (\text{A11})$$

where A_{aper} is the area of the aperture.

The throttle valve can be considered to be an aperture, with a variable slit width defined as

$$d_{\text{slit}} = d_{\text{aper}} \equiv d_{\text{valve}}/U, \quad (\text{A12})$$

where U is the factor by which molecular flow is attenuated by the partially closed throttle valve [determined experimentally with He at low pressures (~ 0.1 mTorr) or with Cl₂ in this study]. Consequently, $C_{\text{valve}}^t(A) [= C_{\text{aper}}^t(A)]$ can be obtained from Eqs. (A9) and (A11), with d_{aper} provided by Eq. (A12) and $A_{\text{aper}} = \pi d_{\text{valve}}^2/4U$.

Transition flow conductance through a short tube [$C_{\text{tube}}^t(A)$] is sometimes treated as a series of conductances through a long tube [Eq. (A11)] and an aperture [$C_{\text{aper}}^t(A)$] [45]:

$$1/C_{\text{tube}}^t(A) = 1/C_{\text{long tube}}^t(A) + 1/C_{\text{aper}}^t(A). \quad (\text{A13})$$

Although Eq. (A13) has the correct asymptotic limits for infinitely long and short tubes, it has been shown to be quite inaccurate (5% error or more) for finite length tubes [46]. Fortunately, the error introduced in computing the relative number densities of the rare gases is negligible because $1/C_{\text{tube}}^t(A)$ is generally smaller than $1/S(A) + 1/C_{\text{valve}}^t(A)$, and similar systematic errors are made for all of the rare gases.

The long tube transitional flow conductance can be expressed as [41]

$$C_{\text{long tube}}^t(A) = C_{\text{long tube}}^v(A) + \left(\frac{\text{Kn}(A) + \sqrt{\pi/2}}{\text{Kn}(A) + 1.235\sqrt{\pi/2}} \right) C_{\text{long tube}}^m(A), \quad (\text{A14})$$

where $C_{\text{long tube}}^v(A)$ is the long tube viscous flow conductance, described by the Poiseuille equation

$$C_{\text{long tube}}^v = \frac{\pi d_{\text{tube}}^4}{256\eta l_{\text{tube}}} (P + P_{\text{valve}}), \quad (\text{A15})$$

where P and P_{valve} are, respectively, the vessel pressure and the pressure at the upstream side of the valve (dyn/cm²). $C_{\text{long tube}}^m(A)$ is the molecular long tube conductance, given by [41]

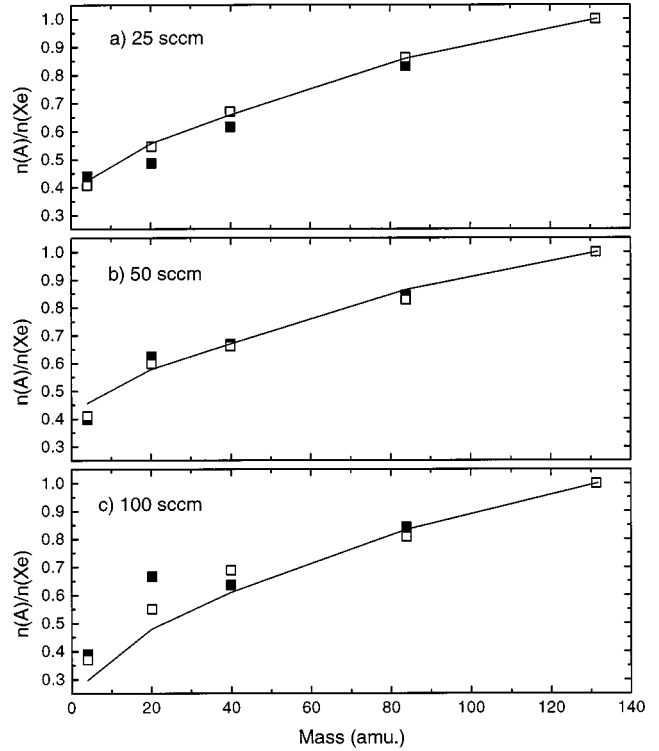


FIG. 15. Number density increases (normalized to the number density increase for Xe addition) measured with the addition of 5 (solid squares) or 10 (open squares) sccm of a single rare gas to a flow of (a) 25, (b) 50, or (c) 100 sccm of Cl₂. The valve was fully open for (a) and (b), and partially closed such that the area of the opening was reduced by a factor of 11 in (c). Solid lines are predictions from the model described in the Appendix.

$$C_{\text{long tube}}^m(A) = \frac{d_{\text{tube}}^3}{3l_{\text{tube}}} \sqrt{\frac{\pi RT_g}{2m_A}},$$

where R is the gas constant.

The coefficient of viscosity, $\eta(A)$, for a single gas is given by

$$\eta(A) = \frac{0.499m(A)v(A)}{\sqrt{2}\pi N_A d(A)^2}, \quad (\text{A16})$$

where $m(A)$ is the molecular weight of the gas and N_A is Avagadro's number. For a mixture of n gases, the viscosity is given by [47]

$$\eta = \frac{\sum_{i=1}^n x_i \eta_i}{\sum_{j=1}^n x_j \phi_{ij}}, \quad (\text{A17})$$

where x_i is the fraction of each gas and

$$\phi_{ij} = \frac{1}{\sqrt{8}} \left(1 + \frac{m_i}{m_j} \right)^{-1/2} \left[1 + \left(\frac{\eta_i}{\eta_j} \right)^{1/2} \left(\frac{m_j}{m_i} \right)^{1/4} \right]^2, \quad (\text{A18})$$

with m_i and m_j being masses. For computations of the relative number densities of each of the rare gases in the small amount of the mixture added to Cl₂, the viscosity of Cl₂ can be used with a negligible error. However, when computing

the pressure rise caused by adding a small amount (say, 5% or 10%) of one rare gas to Cl_2 (as will be done below to compare model predictions with measurements), the small change in the viscosity caused by the added rare gas will cause a change in the viscous flow conductance that is comparable to the pressure rise expected from the addition of the rare gas [$\sim f(A)/f(\text{Cl}_2)$]. The percent change in pressure caused by the change in the viscous flow conductance will in turn approach the percent change in the viscous flow conductance when this flow regime dominates (at very high flow rates and high pressures, with the valve mostly opened). Therefore, the viscosity of the two component mixture must be used in these cases. Equations (A15) and (A16) are kept in the simpler form to be used with the five-component mixture, with A being Cl_2 in Eq. (A16), $\eta \approx \eta(\text{Cl}_2)$, and P and P_{valve} being Cl_2 pressures.

The pressure above the valve is given by

$$P_{\text{valve}}(A) = RTf(A)[1/S(A) + 1/C'_{\text{valve}}(A)]. \quad (\text{A19})$$

$P_{\text{valve}}(\text{Cl}_2)$ is obtained from Eq. (A19) and used to obtain $C_{\text{long tube}}^V$ from Eq. (A15) with $\eta \approx \eta(\text{Cl}_2)$. $C_{\text{long tube}}^V$ is then used with the equations above that are specific to the different gases to compute number densities of the five rare gases. These values are used in the calculation of electron temperatures by the TRG-OES method.

Before giving correction factors for the rare gases under some representative conditions, we present some closely related computed number density rises when a single rare gas is added to Cl_2 . The model predictions are compared with experimental measurements in Fig. 15, for three Cl_2 flow rates. The model is in good agreement with the measurements.

Finally, number densities were computed for all of the conditions used in this study. The extremes of these values are presented in Table II, normalized to the Xe number density to obtain the correction factors by which the number densities of Kr and Ar should be multiplied by to correct for these gas flow effects.

-
- [1] N. Fujiwara, T. Maruyama, M. Yoneda, K. Tsukamoto, and T. Banjo, *Jpn. J. Appl. Phys., Part 1* **33**, 2164 (1994).
- [2] N. Fujiwara, T. Maruyama, and M. Yoneda, *Jpn. J. Appl. Phys., Part 1* **34**, 2095 (1995).
- [3] S. Samukawa, *J. Appl. Phys.* **33**, 2133 (1994).
- [4] S. Samukawa, Y. Nakagawa, T. Tsukada, H. Ueyama, and K. Shinohara, *Jpn. J. Appl. Phys., Part 1* **34**, 6805 (1995).
- [5] M. V. Malyshev, V. M. Donnelly, S. W. Downey, J. I. Colonell, and N. Layadi (unpublished).
- [6] I. Langmuir, *Gen. Electr. Rev.* **26**, 731 (1923).
- [7] V. A. Godyak (unpublished).
- [8] N. Hershkowitz, in *Plasma Diagnostics*, edited by O. Auciello and D. L. Flamm (Academic, New York, 1989), Vol. 1.
- [9] M. V. Malyshev, V. M. Donnelly, A. Kornblit, N. A. Ciampa, J. I. Colonell, and J. T. C. Lee, *J. Vac. Sci. Technol. A* **17**, 480 (1999).
- [10] M. D. Bowden, T. Okamoto, F. Kimura, H. Muta, K. Uchino, K. Muraoka, T. Sakoda, M. Maeda, Y. Manabe, M. Kitagawa, and T. Kimura, *J. Appl. Phys.* **73**, 2732 (1993).
- [11] K. L. Junck and W. D. Getty, *J. Vac. Sci. Technol. A* **12**, 2767 (1994).
- [12] T. Mehdi, P. B. Legrand, J. P. Dauchot, M. Wautelet, and M. Hecq, *Spectrochim. Acta B* **48**, 1023 (1993).
- [13] Y. Nakamura, M. Wong, and I. Matsui, in *Proceedings of the 11th International Conference on Gas Discharges and Their Applications, Tokyo, 1995* (Inst. Elec. Eng. Japan, Tokyo, 1995), p. II-402.
- [14] A. A. Shatas, Y. Z. Hu, and E. A. Irene, *J. Vac. Sci. Technol. A* **10**, 3119 (1992).
- [15] D. A. O. Hope, T. I. Cox, and V. G. I. Deshmukh, *Vacuum* **37**, 275 (1987).
- [16] M. V. Malyshev and V. M. Donnelly, *J. Vac. Sci. Technol. A* **15**, 550 (1997).
- [17] M. V. Malyshev, V. M. Donnelly, and S. Samukawa, *J. Appl. Phys.* **84**, 1222 (1998).
- [18] H. L. Maynard, M. V. Malyshev, V. M. Donnelly, and W. W. Tai (unpublished).
- [19] V. M. Donnelly, M. V. Malyshev, A. Kornblit, N. A. Ciampa, J. I. Colonell, and J. T. C. Lee, *Jpn. J. Appl. Phys., Part 1* **37**, 2388 (1998).
- [20] M. V. Malyshev, Ph.D. thesis, Princeton University, 1999.
- [21] N. C. M. Fuller, M. V. Malyshev, V. M. Donnelly, and I. P. Herman (unpublished).
- [22] J. T. Fons and C. C. Lin, *Phys. Rev. A* **58**, 4603 (1998).
- [23] M. A. Lieberman and A. J. Lichtenberg, *Principles of Plasma Discharges and Materials Processing* (Wiley, New York, 1994).
- [24] J. E. Chilton, J. B. Boffard, R. S. Schappe, and C. C. Lin, *Phys. Rev. A* **57**, 267 (1998).
- [25] P. V. Feltsan and I. P. Zapesochnyi, *Ukr. Fiz. Zh. (Russ. Ed.)* **12**, 1423 (1967).
- [26] M. V. Malyshev and V. M. Donnelly (unpublished).
- [27] J. B. Boffard, G. A. Piech, M. F. Gehrke, L. W. Anderson, and C. C. Lin, *Phys. Rev. A* **59**, 2749 (1999).
- [28] A. A. Mitureva, N. P. Penkin, and V. V. Smirnov, *Opt. Spectrosc.* **67**, 785 (1989) [*Opt. Spectrosc.* **67**, 461 (1989)].
- [29] A. A. Mitureva and V. V. Smirnov, *Opt. Spectrosc.* **74**, 12 (1993) [*Opt. Spectrosc.* **74**, 6 (1993)].
- [30] C. Winstead and V. McCoy (unpublished).
- [31] E. L. Lewis, *Proc. Phys. Soc. London* **92**, 817 (1967); P. G. Wilkinson, *Can. J. Phys.* **45**, 1715 (1967); D. K. Anderson, *Phys. Rev.* **137**, 21 (1965); E. Ellis and N. D. Twiddy, *J. Phys. B* **2**, 1366 (1969); R. Turner, *Phys. Rev.* **140**, 426 (1965); **158**, 121 (1967).
- [32] E. V. Karoulina and Y. A. Lebedev, *J. Phys. D* **25**, 401 (1992).
- [33] A. Bogaerts and R. Gijbels, *Phys. Rev. A* **52**, 3743 (1995).
- [34] D. P. Lymberopoulos and D. J. Economou, *J. Appl. Phys.* **73**, 3668 (1993).
- [35] S. Rauf and M. J. Kushner, *J. Appl. Phys.* **82**, 2805 (1997).
- [36] E. J. McGuire, *Phys. Rev. A* **20**, 445 (1979).
- [37] J. O. Hirschfelder, C. F. Curtis, and R. B. Bird, *Molecular Theory of Gases and Liquids* (Wiley, New York, 1967).
- [38] M. V. Malyshev, V. M. Donnelly, A. Kornblit, and N. A. Ciampa, *J. Appl. Phys.* **84**, 137 (1998).
- [39] M. V. Malyshev, N. C. M. Fuller, K. H. A. Bogart, V. M. Donnelly, and I. P. Herman, *Appl. Phys. Lett.* **74**, 1666 (1999).

- [40] Actually, we need to consider only the metastable states (and in some cases low-lying radiative $1s2$ and $1s4$ states), since the density of all $2p$, $3p$, and higher levels is much smaller than the metastable density due to very rapid radiative decay.
- [41] *Foundations of Vacuum Science and Technology*, edited by J. M. Lafferty (Wiley, New York, 1998).
- [42] K. H. Bernhardt, *J. Vac. Sci. Technol.* **1**, 136 (1983).
- [43] J. Kieser and M. Grundner, *Vide* **201**, 376 (1980).
- [44] F. T. Wall, *Chemical Thermodynamics* (Freeman, San Francisco, 1965).
- [45] F. A. O'Hanlon, *J. Vac. Sci. Technol. A* **5**, 98 (1987).
- [46] J. F. O'Hanlon, *A User's Guide to Vacuum Technology* (Wiley, New York, 1980).
- [47] R. B. Bird, W. E. Stewart, and E. N. Lightfoot, *Transport Phenomena* (Wiley, New York, 1960).